PERGAMON

International Journal of Multiphase Flow 25 (1999) 1243–1262

International Journal of Multiphase Flow

www.elsevier.com/locate/ijmulflow

Nonlinear rivulet dynamics during unstable wetting flows

David T. Moyle, M.-S. Chen, G.M. Homsy*

Department of Chemical Engineering, Stanford University, Stanford, CA 94305-5025, USA

Received 1 September 1997; received in revised form 31 May 1999

Personal prologue (GMH): I first met Gad Hetsroni during one of his visits to Stanford in the early 1970s. While the precise date is uncertain, he was 'drumming up business' for the newly launched *International Journal of Multiphase Flow*. He was obviously successful in 'drumming' on Andy Acrivos, as a nice paper by Barthes and Acrivos begins volume 1, page 1. [It is no surprise that he was successful — as all the contributors to this special volume know full well, almost everything Gad decides is good for the journal and for the field of multiphase flow is successful by force of his conviction and personality.] My first papers in the journal were in the mid-1970s. In the process of normal editorial correspondence, I was very quickly 'introduced' to the Hetsroni obsession with *inclusive* page numbers in all citations! I remember being puzzled at this, which struck me as a bibliographical detail. It was only later that I came to appreciate it as a manifestation of the 'pride of ownership' of the journal that drives Gad to make sure that both content and presentation are of the highest quality possible. It was also around that time that he started to hold his short course on multiphase flow at Stanford which meant that he was a frequent and welcomed visitor in the late 1970s and early 1980s. He even enticed me to lecture in one of these courses — the trauma of preparing 'slide notes' is one that has only recently begun to fade in my memory! His many subsequent visits all had the Hetsroni hallmark — an abrupt, unannounced phone call (and more recently, cryptic email messages) running something like this: 'Hello, I'm coming tomorrow and can meet with you at 2:00'. I got to the point where I just assumed that a caller not identifying himself *had* to be Gad. (At least the email headers give some warning....) One of the more recent of these carried an invitation to serve on the editorial board of the Journal, which I immediately accepted. It represents a continuation of a very pleasant personal and professional association that has spanned over 25 years. Gad has promulgated an interest in multiphase flow problems with unusual tenacity, clarity of vision, and singleminded focus, and it is a pleasure to be able to contribute the following paper to this special volume on the occasion of his 65th birthday.

Abstract

The growth and propagation of nonlinear rivulets is studied. Lubrication theory and a Navier type slip model are used to establish the thin film equation for the nonlinear evolution of the height of liquid in the vicinity of a driven contact line. This equation is then solved using a semi-implicit numerical scheme, adapted to handle the moving boundary nature of the problem. The problem involves two parameters, α, a dimensionless slip parameter and the dimensionless contact slope $C = (3Ca)^{-1/3}\tan(\theta)$,

* Corresponding author.

PII: S0301-9322(99)00062-2

where θ is the contact angle and Ca is the capillary number, $\mu U/\sigma$. A parametric study establishes both the shapes and the dynamics of nonlinear rivulet propagation. The shapes are found to be relatively independent of the slip parameter and are primarily determined by the contact slope, while the rivulet speeds are dependent on the level of slip, as expected. The computed shapes, including the occurrence of a capillary bulge near the advancing front, are in excellent agreement with experiments. Chevron-shaped steady traveling wave solutions, and both chevron and straight-sided convectively propagating shapes are obtained, with the traveling wave solutions occurring for small contact slope and the straightsided solutions for large slope. Complete coating of the substrate in the presence of rivulet instabilities occurs only for $C > 1.0$. The predictions are in excellent agreement with experiments and suggest that simple lubrication theory and slip models are all that is necessary to describe the observed shapes and dynamics.

Keywords: Dynamic contact lines; Rivulets; Instabilities

1. Introduction

Huppert (1982) first described the instability of a driven contact line in an experimental study of gravity driven wetting dynamics. An initially straight dynamic contact line becomes unstable to spanwise variations in its height, position and speed, leading to the propagation of nonlinear rivulets which in many cases form a nearly periodic array in the spanwise direction. Huppert described the propagation characteristics of the front before the instability manifests itself in terms of a balance between gravitational driving and viscous resistance. Further scaling arguments suggested that surface tension is important near the contact line. Huppert's data on the wavelength of the rivulets supported the hypothesis that the fingering occurred on the capillary length scale, and therefore the instability was hydrodynamic in origin. Since that time, there has been a thorough exposition of both the features of the steady one-dimensional profiles and their linear stability properties: see e.g. Troian et al. (1989) and Spaid and Homsy (1996).

It has been established that the regions near the contact line are those in which surface tension, viscosity and the driving body force are equally important, and that inner solutions near the contact line may be determined independently of the outer solution to which they match (Troian et al., 1989; Goodwin and Homsy, 1991). It is further found that the particular model used to relieve the contact line singularity leads to only minor differences in the computed one dimensional solutions (Tuck and Schwartz, 1990; Spaid and Homsy, 1996). Both lubrication theory, valid for small slope (Troian et al., 1989; Tuck and Schwartz, 1990; Spaid and Homsy, 1996), and numerical solutions of the Stokes flow equations (Goodwin and Homsy, 1991) show features in common, in particular the occurrence of standing capillary waves and the presence of a capillary ridge, the latter being intimately connected to the mechanism of instability (Spaid and Homsy, 1996).

The linear stability of these one-dimensional solutions has been analyzed by standard techniques, but only in the range of parameters for which lubrication theory is valid. These analyses show that the wave length of the instability scales with the capillary length and is very weakly dependent on the contact line model, but that the growth rate is parameter dependent,

generally increasing with decreasing slip length and/or precursor film thickness (Troian et al., 1989; Spaid and Homsy, 1996). Although some experiments show deviation (de Bruyn, 1992), the predictions of linear theory of both the wave length and the growth rate of the instability have been generally verified in works by Troian et al. (1989), Melo et al. (1989), Fraysse and Homsy (1994), Goodwin (1991) and Spaid and Homsy (1997).

Our interest is in the propagation features of strongly nonlinear rivulets, which are characterized by the following features. First, the presence of a capillary ridge persists in most circumstances, although it is distorted by the fact that the tip of the rivulet has finite spanwise curvature. Fluid still piles up against the action of surface tension in a fashion that is analogous to the one dimensional case (Goodwin, 1991, Johnson et al., 1996). Second, the rivulet takes on one of two nonlinear shapes which are sketched in Fig. 1. In the first of these, the sides of the rivulet are chevron or triangular shaped, and the leading and trailing parts of the contact line, referred to in this paper as the 'peak' and the 'trough', are seen to travel at the same speed, leading to a *nonlinear steady traveling wave solution* in a moving frame. In the second shape, the rivulet sides are straight, i.e., aligned in the flow direction, the trough comes to a halt, and the peak continues to propagate at finite speed, leading to a *convective spreading* of the distance between peak and trough. Clearly the substrate is completely coated in the first case and not in the second. The conditions under which these two cases occur are of obvious technological interest in coating applications.

Huppert (1982) observed these two basic shapes in his original studies by changing the fluids rather than the substrate material. In doing so, he changed both contact angle and capillary number (through the change in surface tension), and although the wavelength of the initial instability scaled with capillary number in the expected fashion, the dependence of the nonlinear rivulet shape on the parameters of the problem remained unknown. The issue was further studied and definitive experimental results obtained by Silvi and Dussan V. (1991), who

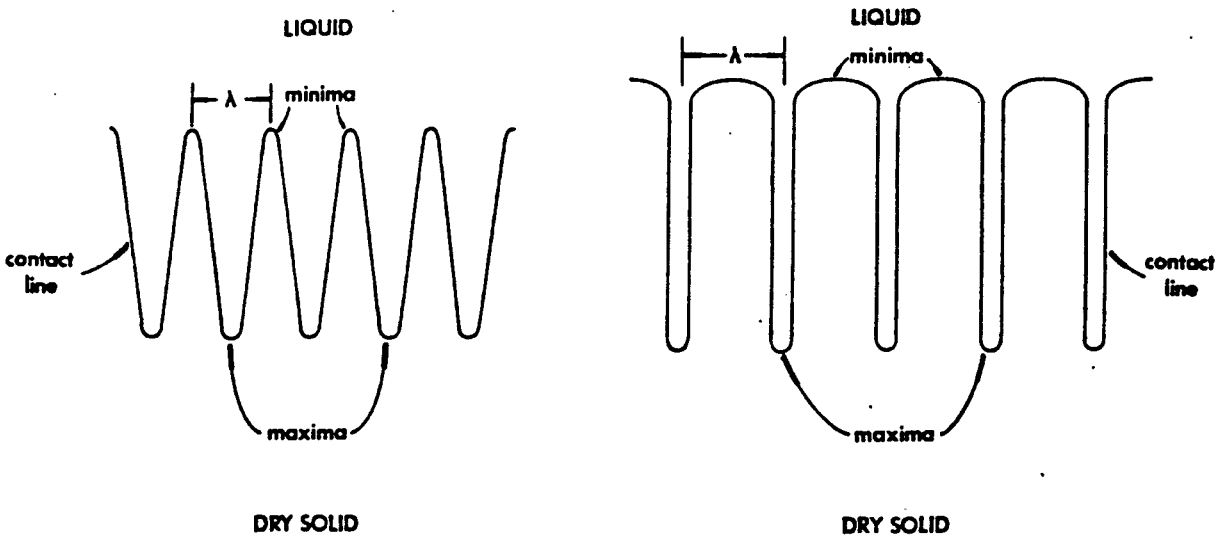

Fig. 1. Sketch of the two different types of nonlinear rivulet propagation that have been observed after Silvi and Dussan V. (1991).

changed substrate materials while keeping the fluid and all other conditions constant, and succeeded in observing *both* nonlinear shapes with the *same fluid*. In this way, they concluded that the contact angle was the main determinant of which shape will be observed. The dependence of the shape on such parameters as the contact angle and capillary number, and whether or not models that involve dynamic contact angles must be used in order to explain the experiments, are still open questions.

The objectives of the present work are to predict the nonlinear propagation properties and rivulet shapes as functions of the parameters, and to assess the ability of simple slip models with constant contact angle to describe the experimental observations. The only previous work we know of, is that of Schwartz (1989), who was able to simulate the qualitative features of nonlinear rivulet propagation using a precursor film model appropriate to a completely wetting fluid of zero contact angle. His short study succeeded in predicting the chevron type pattern seen in experiments with wetting fluids. The use of the precursor film model, however, precludes any study of the effect of contact angle on nonlinear shape. The present paper specifically addresses this issue by adopting a slip model, allowing the specification of the contact angle as a parameter.

Section 2 of the paper gives the basic equations to be solved, together with a discussion of the slip model used and the resulting dimensionless parameters. Features of the steady one-dimensional solutions and their stability characteristics are briefly reviewed. Section 3 describes our numerical method, the most complicated part of which requires the implementation of logic associated with determining the approximate position of the contact line, following a numerical time step. Validation studies are also reported in this section. Section 4 gives our main results in the form of a parametric study of nonlinear rivulet shape as a function of the parameters and a comparison with experiments. We mention that while our discussion and comparison is with gravity-driven motion down an inclined plate, the formulation, solution technique, and conclusions apply more generally to the class of contact line instabilities driven by any body force. In particular, our conclusions certainly apply to spin coating (Melo et al., 1989; Fraysse and Homsy, 1994), and probably to more general surface shear driven spreading problems as well. The paper ends with a short section, Section 5 containing our conclusions.

2. Basic equations

Fig. 2 shows the definition sketch in which a contact line is driven at speed U by an imposed body force in the positive x direction. The liquid has viscosity μ and surface tension σ. The height of the liquid is given by $y = h(x,z,t)$. If the front is straight, h is independent of z and we refer to this as the 'one-dimensional solution'. This is the quasistatic base state solution, which is susceptible to a spanwise instability leading to rivulet formation.

In this paper we make two standard assumptions. The first is that surface tension is important only in the immediate vicinity of the contact line. The second is that lubrication theory can be used to describe the flow in the thin film, whose interfacial position is of uniformly small slope. The first assumption allows the use of matched expansions in the description of the flow, in which an inner solution near the contact line is asymptotically matched onto an outer solution in which interfacial tension is negligible, but which may be

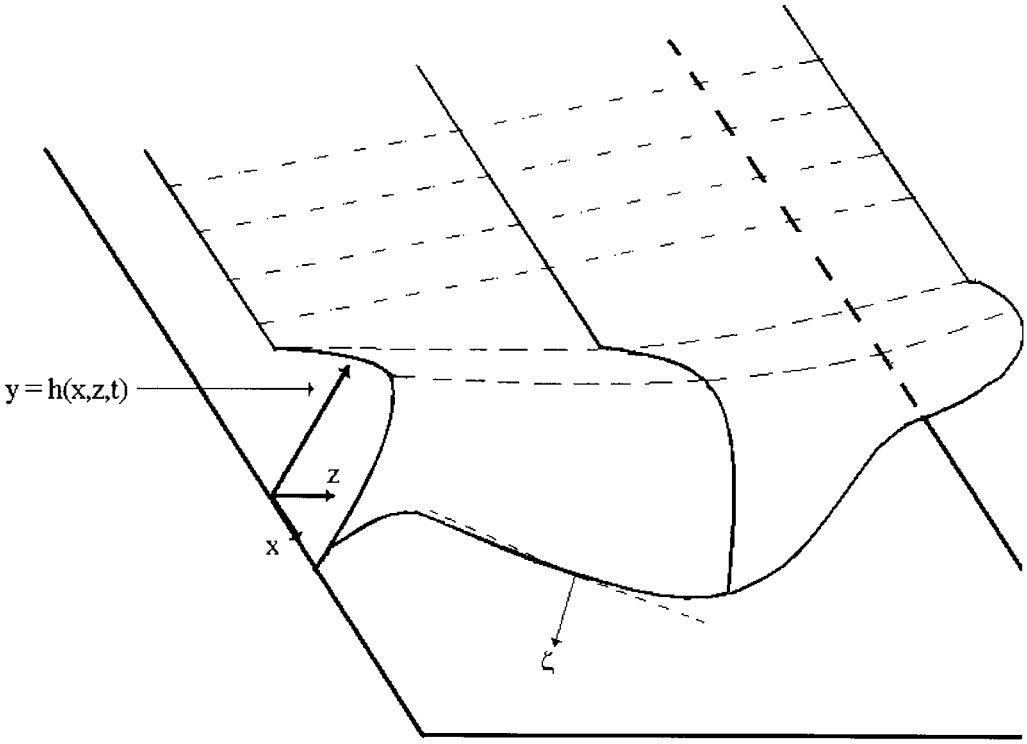

Fig. 2. Schematic of a two-dimensional rivulet and definition sketch.

time dependent, as discussed by Huppert (1982), Troian et al. (1989), and Goodwin and Homsy (1991). The dynamics in the inner region occur on a separate time scale than those in the outer region, leading to matching onto a uniform film thickness scaled to be unity. These and related issues are well discussed in previous papers by Troian et al. (1989) and Goodwin and Homsy (1991), and will not be re-developed here. The second assumption is then valid when $\{(3Ca)^{-1/3}\tan(\theta)\}$ is an $O(1)$ quantity, where Ca is the capillary number and θ is the contact angle. For a discussion, see Goodwin and Homsy (1991).

As is well known, it is necessary to use a model that eliminates the contact line singularity. Two such models, a precursor film model and a Navier slip model, have been used extensively and to good advantage (Tuck and Schwartz, 1990). Since our focus is on the parametric dependence of the nonlinear rivulet shape on the contact angle, we use a model capable of independent specification of the contact angle, i.e. a Navier slip model, as developed by Greenspan (1978), and discussed in this context by Spaid and Homsy (1996) and Tuck and Schwartz (1990). In this model, the no-slip condition is replaced by the condition:

$$u_s = \alpha' \tau / 3h \tag{1}$$

where α' is a dimensional slip parameter, u_s is the tangential velocity at the solid surface, and τ is the tangential stress. It is well known that such a model leads to slip near the contact line where stresses are large and no-slip elsewhere, and the $(1/h)$ thickness dependence of the slip length is the simplest that leads to finite traction at the contact line (Greenspan, 1978).

We do not give a complete derivation of the basic equations here, since their development is well documented by Spaid and Homsy (1996). Using well known scalings and stretchings appropriate to the inner region, the equation governing the *dimensionless* liquid height, $h(x,z,t)$ is:

$$h_t + (1+\alpha)h_x + \left[\left(h^3 + \alpha h\right)(1 + h_{xxx} + h_{xzz})\right]_x + \left[\left(h^3 + \alpha h\right)(h_{xxz} + h_{zzz})\right]_z = 0 \tag{2}$$

In these equations, $h(x,z,t)$ has been scaled with the matching height far from the interface, x is the streamwise coordinate and z the spanwise coordinate, both scaled by the inner scale $(3Ca)^{1/3}$ near the contact line, t is the time scaled appropriately in the inner region, and α is the dimensionless slip parameter.

The boundary conditions on x for Eq. (2) consist of two matching conditions and two contact line conditions. The matching conditions may be easily written as:

$$x \to -\infty \quad h = 1,\ h_x = 0 \tag{3}$$

The contact line conditions require more discussion. Denoting the location of the contact line as $\mathbf{x}_{CL} = (x_{\mathrm{CL}}, y_{\mathrm{CL}})$ and referring to Fig. 2, we denote the local unit normal as ζ. The contact line position is then by definition the point where the height of the liquid vanishes, and at this point, the local tangent plane of the interface must contact the solid at a specified contact angle. These conditions may be written as:

$$\text{at } \mathbf{x} = \mathbf{x}_{\mathrm{CL}}(t) \quad h = 0,\ h_\zeta = C. \tag{4}$$

In these boundary conditions, the parameter C is related to the scaled contact angle as:

$$C = (3Ca)^{-1/3}\tan(\theta). \tag{5}$$

C is referred to here as the contact slope, as it measures the slope of the interface in the scales of the inner region, and is a key parameter of our theory. These boundary conditions are augmented by periodic conditions in z appropriate to a periodic array of identical rivulets (an idealization of the nearly periodic array seen in experiments) and a suitable initial condition at $t = 0$.

As can be seen, our two basic assumptions lead to a nonlinear parabolic partial differential equation for the liquid height. The moving boundary nature of the problem is made clear by Eq. (4) by which the contact line is defined as the locus of points at which $h = 0$. Also, as can be seen, the problem is characterized by two dimensionless parameters, the slip parameter α (related to a slip length) and the scaled contact slope, C. Our task is to solve these equations to obtain the propagation characteristics and the shapes of nonlinear rivulets.

3. Numerical solution

3.1. Numerical algorithm

We use finite difference methods to solve the problem. We do this in two stages: first, by

solving the one-dimensional version of Eq. (2) to obtain the quasistationary state, and then, by imposing a two-dimensional perturbation on this steady state and solving the two-dimensional equations. The algorithm used for the one-dimensional simulations is straightforward and will not be discussed in detail since it is simply the one-dimensional version of the more complicated two-dimensional algorithm described below.

Since the rivulets occur nearly periodically in the experiments, we use periodic boundary conditions in the spanwise direction. As a result of the expected symmetry, it is necessary to simulate only one half a rivulet, i.e. a half-wave length, with an array of rivulets being obtained by reflections of the half-wave solution and periodic extensions. Our code exploits this by using a grid with symmetry planes at either edge of the computational domain, with one edge being the trough and the other, the peak of the rivulet. The peak and trough sides are pre-determined as a result of the forcing present in the initial and boundary data described below.

After extensive experimentation with different approaches including an ADI type scheme, we determined that an x-directed implicit scheme was the best compromise between complexity and accuracy and stability. By an x-directed implicit scheme, we mean a Crank-Nicholson method applied to the highest x derivative in each term in Eq. (2), with standard second-order time stepping. Both the nonlinearities due to the variable coefficients and all the z derivatives are treated explicitly by 'freezing' their values at the previous time step, thus the term 'x-directed implicit scheme'.

The main difficulties in the implementation of a finite difference scheme for this moving boundary problem are in keeping track of the location of the contact line and in applying the contact slope condition. The free boundary condition (4) expresses the fact that the contact line is implicitly defined as the locus of points where the liquid height vanishes with contact slope C. The computational domain is divided into a finite difference mesh with equal mesh spacings. We then keep track of points covered by liquid, called 'active' points, and those which are dry substrate, called 'passive' points. The periodic boundary conditions in the spanwise direction are obviously applied only to the active points. Fig. 3 shows a sketch of the local conditions in the vicinity of a dynamic contact line whose local orientation is not along a coordinate axis. At any given time step, the z (or x) positions of the contact line where it crosses the grid lines of constant x (or z) are saved as a separate array. This results in a relatively equally spaced representation of the position of the contact line. These crossing points are referred to as 'contact points'. At each contact point, the local normal to the contact line may also be determined by simple finite differences. This normal vector determines the direction of movement of contact points, as the contact line evolves in time.

The contact line is then moved explicitly in time as follows. Its position is considered fixed while the liquid height is evolved according to Eq. (2). The numerical integration of Eq. (2) over a time step results in a change of the liquid height at all active points and this new height profile will, in general, violate the condition of specified contact slope. We then move the contact line in the direction of its normal by the distance required to re-adjust the contact slope of the tangent plane to the value required by the boundary condition. This can be easily visualized in one dimension, in which the motion of the contact line corresponds to simply sliding the contact point in the x direction by the amount necessary to readjust the slope to its required value. In two dimensions, there are straightforward but tedious details related to both

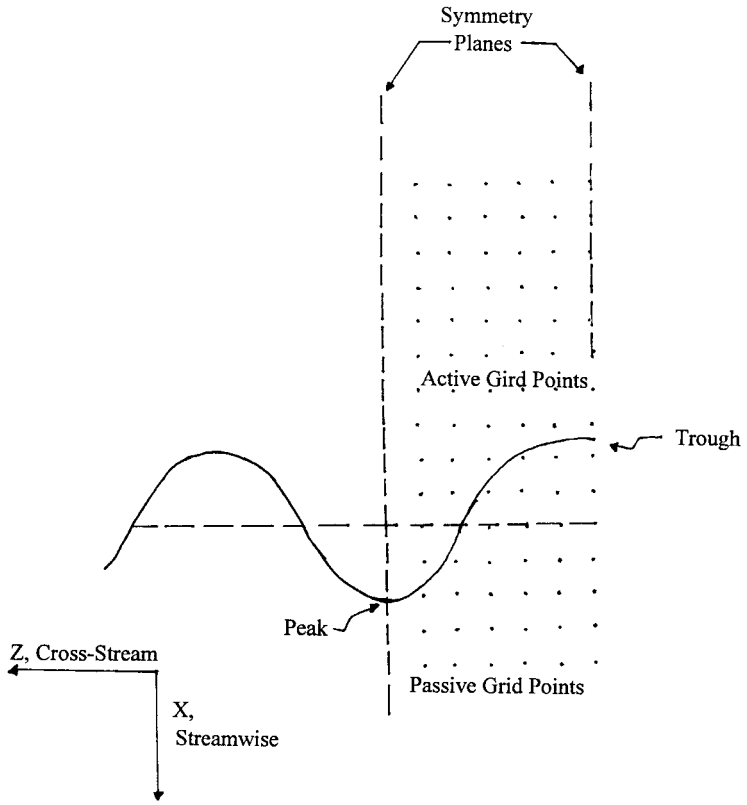

Fig. 3. Sketch of the finite difference grid and the position of a contact line that is not along a coordinate direction.

the interpolation of new height values onto grid points that become active as a result of this movement (which values are required for the next time step), and to the trigonometry associated with computing the contact slope correctly. These details will not be discussed here. The movement of the contact line may result in changes in the state of a mesh point from active to passive or vice versa. A new array of contact points is then constructed. We comment here, that while the adjustment of the location of the contact line may seem like we are allowing numerical slip, this is not the case. As we will show in the validation studies, the faithful adherence of the numerical algorithm to the slip condition requires small time steps so that over one time step the distance moved is consistent with the differential equations, i.e., it is determined by the slip parameter and not by the grid spacing.

The one-dimensional simulations were conducted with a mesh size between 0.01 and 0.005, with the smaller meshes being required for larger contact slope. The two dimensional simulations were conducted with the same resolution in the downstream direction as was found necessary for the one-dimensional solutions, and 15 points over the half-wave in the spanwise direction. This is not to be interpreted as using 15 mesh points over the entire interface. As the rivulet grows in time, many tens to hundreds of points are used to interpolate the interface position, but most of which are axial points. The time step requirements for accuracy and stability were found to be stringent, especially to avoid errors associated with numerical slip.

The time step was varied over an order of magnitude from 2×10^{-4} to 2×10^{-5}. Spot checks of numerical accuracy were made by doubling the number of spanwise points. All simulations were demonstrated to converge with decreasing time step size to an accuracy of greater than 2%. Further quantitative measures of the convergence are given in the validation section below.

3.2. Initial conditions

We conducted two types of simulations: validation studies for the generation of one-dimensional solutions, and two-dimensional simulations of nonlinear rivulets. These are discussed separately below. In the one-dimensional case, we began calculations with a sharp front:

$$h(x,0) = 1 - H(x_i), \tag{6}$$

where H is the Heavyside function and x_i is the initial position of the contact line. We then followed the evolution towards the steady solution.

In the case of the two-dimensional simulations, we began the calculation with a converged one-dimensional solution. Although this solution is linearly unstable, the growth rates are so small that we found it necessary to force the rivulet initially through the imposition of a slight 10% variation in the liquid height far upstream of the contact line for a short duration near the beginning of the simulation. (Remnants of this perturbation may be seen in some of the plots shown in the next section.) This increased fluid flux provided a controlled forcing of the rivulet, and allowed us to set the wavelength of the rivulet as that corresponding to the most unstable wave length according to linear theory, and to pre-determine the position of the peak and trough. This is similar to the study of Schwartz (1989), who also found it necessary to force the growth of the rivulets by an appropriate initial condition.

3.3. Validation studies for one dimensional solutions

We conducted a series of one-dimensional simulations in order to validate the simpler version of our algorithm, especially the manner in which we move the contact line. The equation solved was the one-dimensional version of (2)–(4) above, which for reference are:

$$h_t + (1+\alpha)h_x + \left[\left(h^3 + \alpha h\right)(1 + h_{xxx})\right]_x = 0 \tag{7}$$

with boundary conditions:

$$\text{as } x \to -\infty \quad h = 1,\ h_x = 0, \tag{8a}$$

$$\text{at } x = x_{CL}(t) \quad h = 0,\ h_x = C, \tag{8b}$$

$$\text{at } t = 0, \quad h = 1 - H(x_i). \tag{8c}$$

We note that, similar to the more complicated two-dimensional case, the position of the

contact line is not know a-priori, and is determined as part of the solution by moving it over a time step in a fashion consistent with the prescription of a contact slope C. It can be easily established that a steady state exists in a reference frame traveling with a dimensionless speed $(1+\alpha)$. In addition to obtaining the well-known shape for the steady state profile, the wave speed of the steady solution is also computed as part of the evolution. Hence the agreement between the analytical and numerically determined speeds provides a test of the algorithm for moving the contact line and an indicator of the degree of numerical slip involved.

Fig. 4 shows the time evolution of the solution for the case $\alpha = 0.01$ $C = 2.0$ and a time step of 5×10^{-5}. The solutions were generated in the Eulerian frame, but are displayed in a frame moving with the *analytical* speed of the contact line, $(1+\alpha)$. As expected, the solution evolves from the step profile to a steady solution characterized by the presence of a capillary ridge and decaying standing capillary waves. Also, as is evident, the wave moves with the correct speed, indicating the lack of numerical slip. The solution was also validated by quantitative and qualitative comparison with previous solutions and by mesh refinement. In all cases, the agreement with the speed was to machine accuracy and with the profile was better than 4%.

We generated a family of such one-dimensional steady solutions for the entire range of

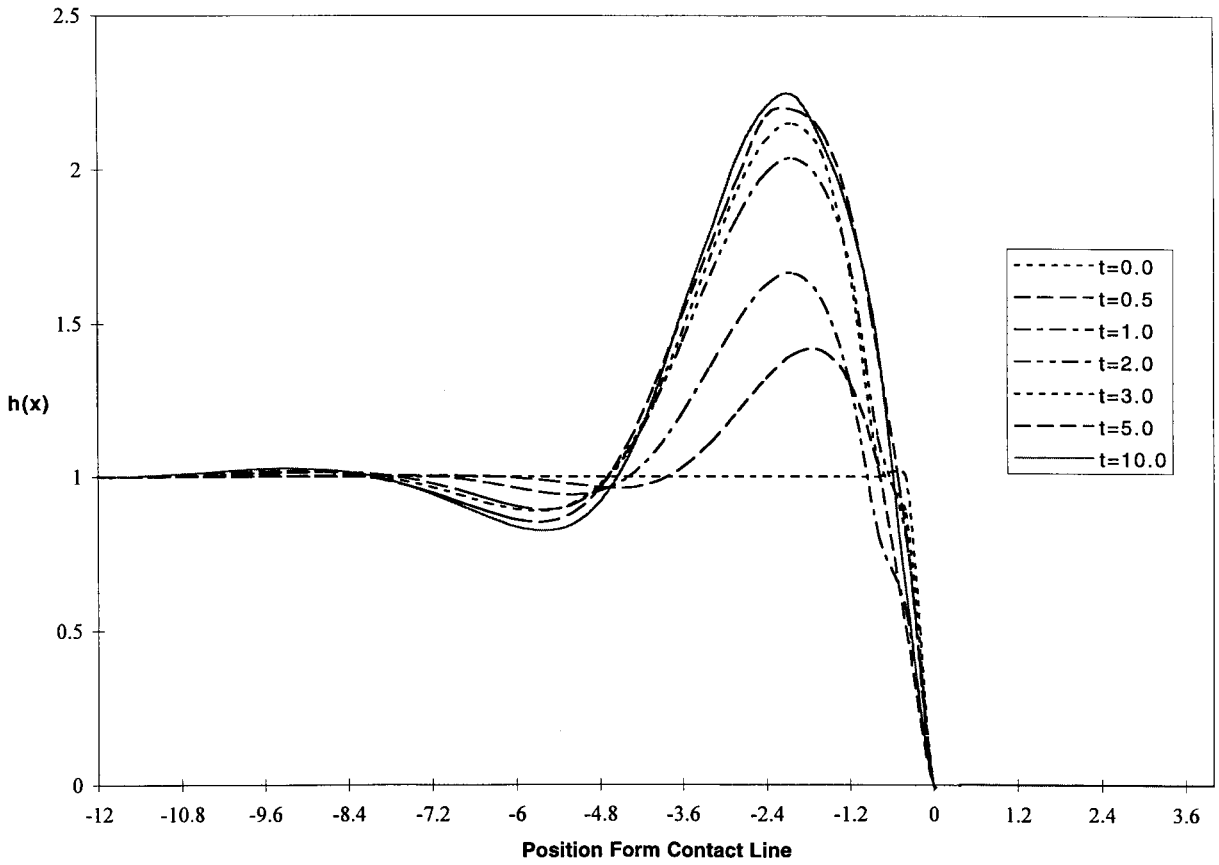

Fig. 4. Time evolution of the one-dimensional solution for the case $\alpha = 0.01$, $C = 2.0$.

parameters α,C reported below. As mentioned above, these solutions were perturbed in the spanwise direction and served as the initial conditions for the two-dimensional solutions reported below.

4. Two-dimensional results and discussion

4.1. Rivulet shapes, propagation modes and dynamics

We have conducted numerical simulations for two values of the dimensionless slip parameter, α, of 0.5 and 0.01, and a range of contact slopes, C. In principle, α should take as small a value as possible, since it represents the range over which significant departure from no-slip occurs, and is in general related to the ratio of microscopic to macroscopic length scales (Greenspan, 1978). We have found little dependence of the results for the rivulet shapes on α, and all our conclusions regarding shapes are robust with regard to the variation with α. Accordingly, we focus on the parametric dependence on C, which we vary over an order of magnitude, i.e. $0.2<C<2.0$. All our results are displayed as two wavelengths of a periodic array of rivulets: (recall that only a half-wave length of the solution is actually computed). The wavelength is chosen as that which has the highest linear growth rate (a wave number of approximately 0.5 in the inner scales), and all results are presented in the Eulerian frame.

Fig. 5(a) shows a typical result of a rivulet shape for the case $\alpha = 0.01$, $C = 2.0$, i.e. the same parameters as in Fig. 4, after a long-time simulation. As can be noted, the sides are essentially straight, and the flux of fluid is carried almost entirely through the rivulet, which is correspondingly higher than the one-dimensional liquid film behind it in order to accommodate this flux. Fig. 5(b) shows the rivulet at the same value of $C = 2.0$ but for a larger value of $\alpha = 0.5$. As expected, the increased slip leads to an increased speed of propagation of the rivulet, as discussed above. Fig. 5(b) also shows the piling up of fluid in a two dimensional capillary bulge seen in recent experiments (Goodwin, 1991; Johnson et al., 1996). Fig. 5(a) and (b) together demonstrate the relative weak dependence of the *type* of rivulet shape on the extent of slip that is typical of all our results.

We find that our simulations mimic the experimental observations in the sense that there are three broad classes of rivulet shapes: chevron or triangular shapes that represent steady traveling wave solutions; chevron shapes, in which the peak moves faster than the trough; and straight-sided shapes in which the peak advances and the trough remains stationary. Figs. 6 and 7 show time evolutions leading to the traveling wave and straight-sided shapes, respectively. In the figures, only the 'active' parts of the computational grid are shown. Fig. 6 shows the time evolution to the long time state of Fig. 5 for $\alpha = 0.01$ and a relatively large value of $C = 2.0$. We clearly see the evolution of the pattern to nonlinear equilibrated structures with straight sides in which the troughs remain stationary and the peaks continue to move down the substrate. These are seen to be very similar in size and shape to those observed experimentally for moderate contact angle fluid/substrate pairs (Huppert, 1982; Silvi and Dussan V., 1991). Fig. 7, which is for the same value of $\alpha = 0.01$, but for a smaller value of $C = 0.2$, shows the evolution typical of lower contact slopes. After an initial transient, the rivulet quickly evolves into a chevron shape, which then propagates without further change in

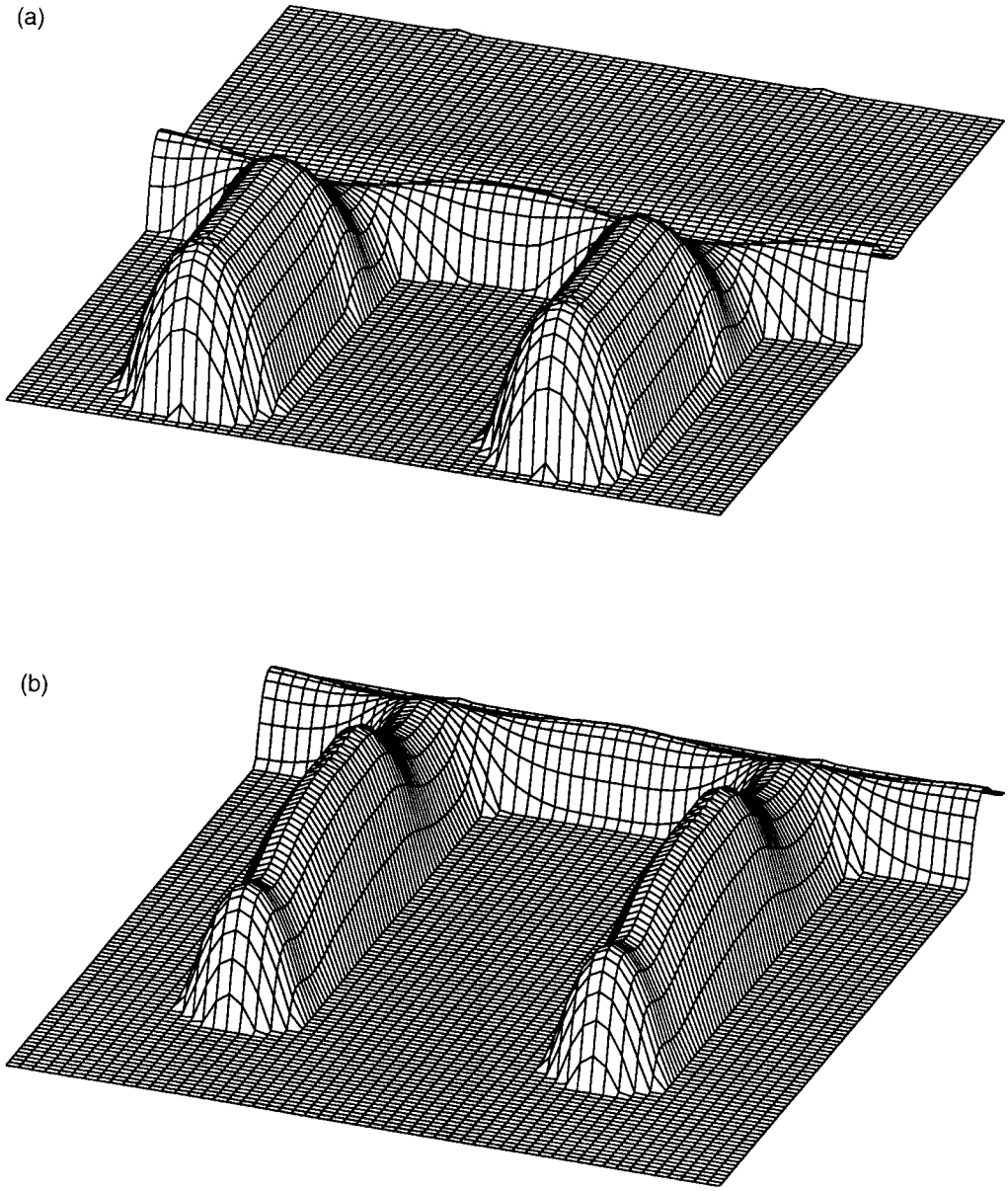

Fig. 5. (a) The nonlinear rivulet shape for the case $\alpha = 0.01$, $C = 2.0$ after a dimensionless time of 50. The corresponding one-dimensional solution is shown in Fig. 4. The finite amplitude rivulet, the sides of which are nearly straight, has equilibrated, the capillary ridge has distorted and the fluid flux is now completely channeled through the peak of the rivulet, and the trough remains dynamically passive; (b) The finite amplitude rivulet for $\alpha = 0.5$, $C = 2.0$: the rivulet is straight-sided, illustrating the weak dependence of the shape on the parameter α.

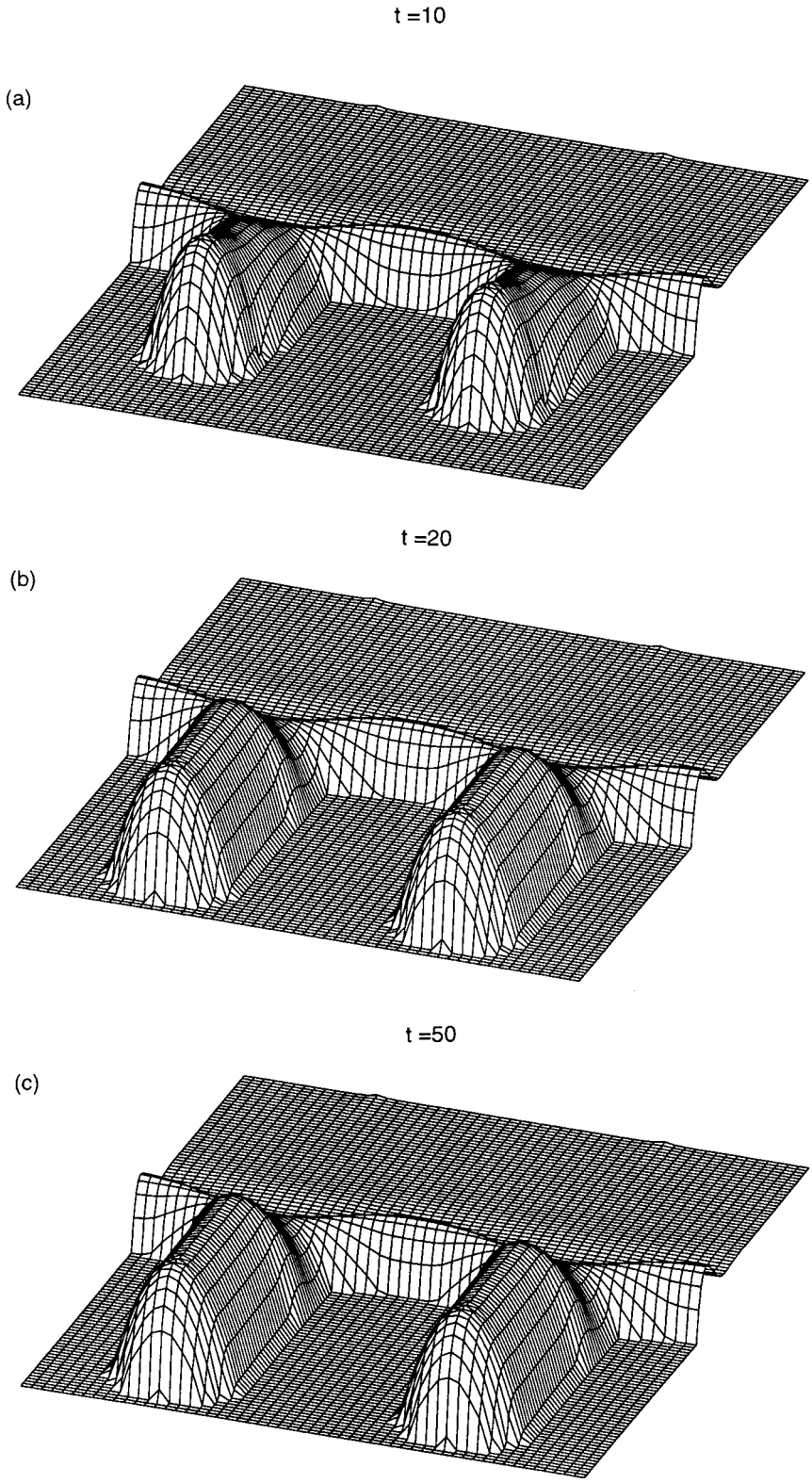

Fig. 6. Time sequence of two-dimensional simulations leading to a straight-sided convectively spreading rivulet. $\alpha = 0.01$, $C = 2.0$, as in Fig. 5: (a) $t = 10$, (b) $t = 20$ and (c) $t = 50$.

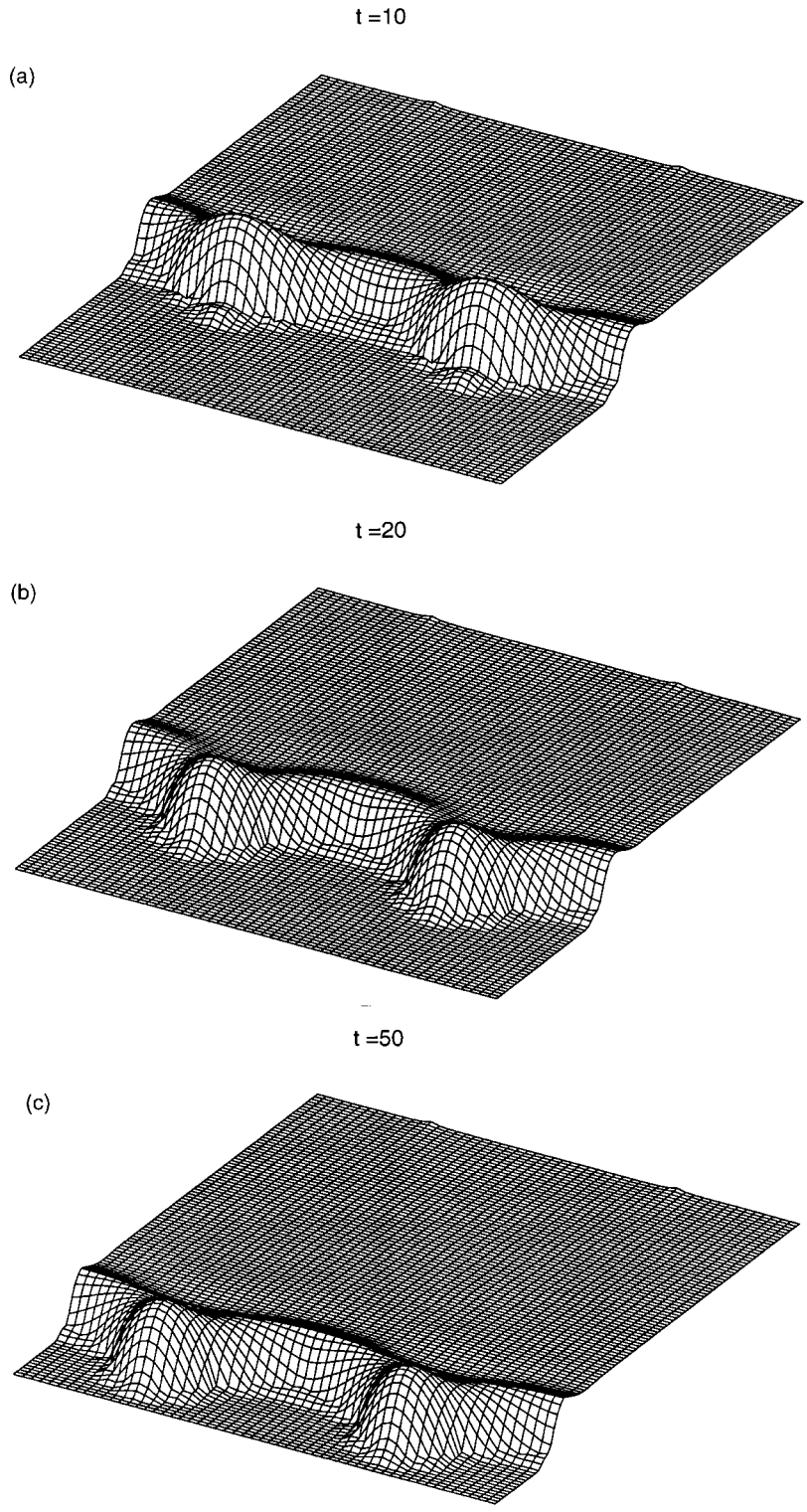

Fig. 7. Time sequence of two-dimensional simulations leading to a traveling wave, chevron-shaped rivulet: $\alpha = 0.01$, $C = 0.2$. (a) $t = 10$, (b) $t = 20$, and (c) $t = 50$.

shape, with both the peak and trough advancing over the substrate. This represents the other class of experimental shapes generally observed for low contact angle fluid/substrate pairs by Huppert (1982), and Silvi and Dussan V. (1991).

Parametric studies have demonstrated that the contact slope, C, is the main determinant of rivulet shape, with chevron-shaped traveling wave solutions obtaining for small C, and straight-sided convectively spreading solutions for large C. These trends are consistent with the study of Schwartz (1989), who found chevron-shaped solutions in the limiting case of $C = 0$, (zero contact angle), and who, in some unpublished work, also observed straightsided rivulets for finite contact angle. Fig. 8 shows the results of a parametric study in C, in which the rivulet shapes for $C = 0.4$, 0.8, 1.0, and 1.2 are shown at a fixed time of $t = 50$. As can be seen, there is a continuous evolution of the shapes from chevrons to straight-sided as C increases, eventually reaching a state in which the trough is stationary and the sides are absolutely straight. This behavior is further quantified in Table 1, in which we record the Eulerian propagation speed of both the rivulet peak and trough for all the parameter values studied. As can be seen, for $C<0.2$, the peak and trough speeds are identical and the corresponding shapes are chevrons. For C between 0.2 and 1.0, the shapes remain chevrons, but the trough moves at a lower speed than the peak, leading to a relative advancement of the leading part of the rivulet. However, since the trough still retains a finite velocity, the substrate will ultimately be

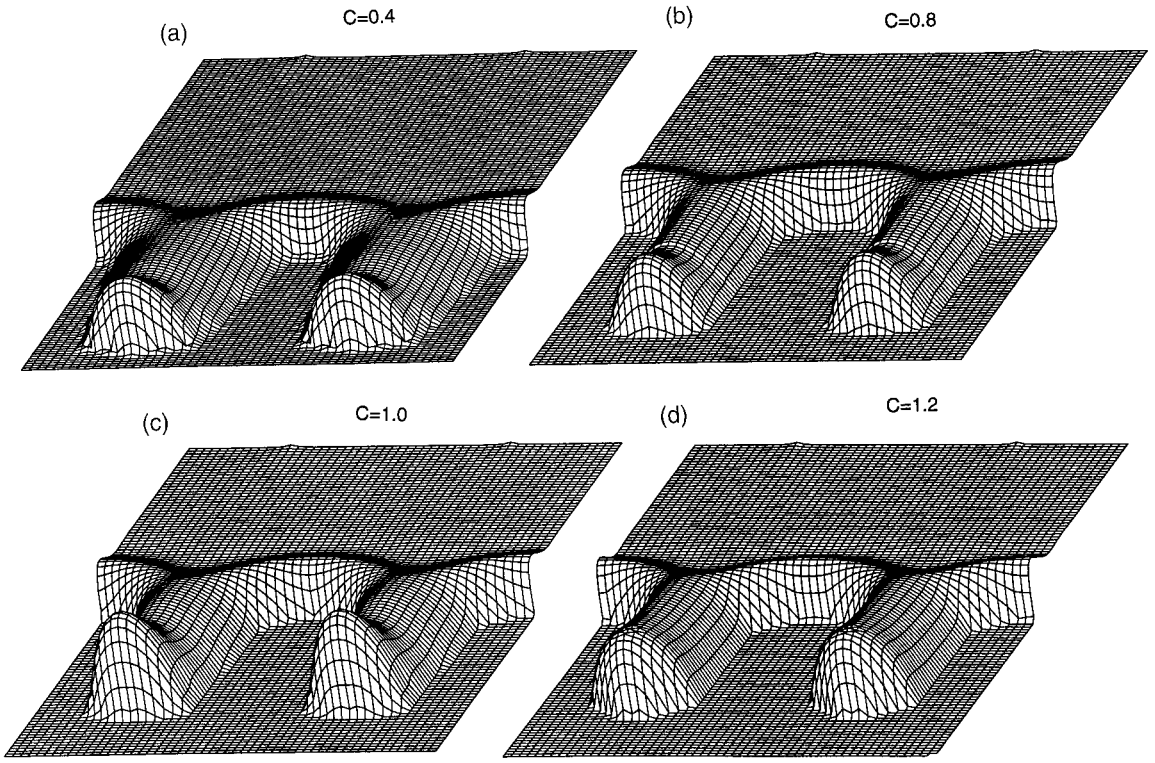

Fig. 8. Parametric study showing the rivulets for fixed $\alpha = 0.01$ and at fixed time $t = 50$, with C as a parameter: (a) $C = 0.4$, (b) $C = 0.8$, (c) $C = 1.0$, and (d) $C = 1.2$.

Table 1
Dimensionless speed of peak and trough location as a function of C for fixed $\alpha = 0.01$

C	Velocity of peak	Velocity of trough
0.2	0.27	0.27
0.4	0.24	0.19
0.6	0.11	0.04
0.8	0.11	0.01
1.0	0.14	0.0
1.2	0.16	0.0
1.4	0.19	0.0
1.6	0.22	0.0
1.8	0.26	0.0
2.0	0.29	0.0

coated with liquid at large times. The trough velocity continues to drop until it vanishes for values of $C > 1.0$. Simultaneously, the shapes undergo an evolution from chevrons to straight-sided rivulets.

We conclude from these studies that the contact angle is the main factor in determining the rivulet shape in experiments in which the capillary number is approximately constant, in agreement with the experiments of Silvi and Dussan V. (1991). But as the theory clearly shows, within the range of validity of our assumptions, the determining parameter is actually the contact slope, $C = (3Ca)^{-1/3}\tan(\theta)$, which is a combination of contact angle and capillary number. Accordingly, care must be exercised in drawing general conclusions from experiments such as those of Silvi and Dussan V., who varied the contact angle while holding Ca approximately constant.

4.2. Comparison with experiments

Goodwin (1991) and Johnson et al. (1996) both conducted experiments on rivulet instabilities in which they used optical techniques to measure the film thickness as a function of both space and time. Shown in Fig. 9 is a typical contour plot of film thickness for glycerine on glass measured by Goodwin (1991). The measurements of Johnson et al. (1996), for a 50% glycerine/water solution on glass, although conducted at finite Reynolds numbers, are similar in all respects. The similarity of the experiments with our simulations, such as those shown in Figs. 5(b) and Fig. 8, is immediately apparent. The capillary ridge has formed a two-dimensional bulge near the advancing peak, the sides of the rivulet are straight, and the cross section of the rivulet is dome-shaped.

We compare the predicted parametric dependence of the families of shapes with the experiments of Huppert (1982) and Silvi and Dussan V. (1991) in an approximate fashion as follows. Both papers record all the fluid properties required to compute the contact slope, $C = (3Ca)^{-1/3}\tan(\theta)$, except for the speed of advance of the contact line. Since both experiments used a fixed amount of starting fluid, this speed is time-dependent, as discussed in Goodwin and Homsy (1991). As explained in Fraysse and Homsy (1994), we need the onset

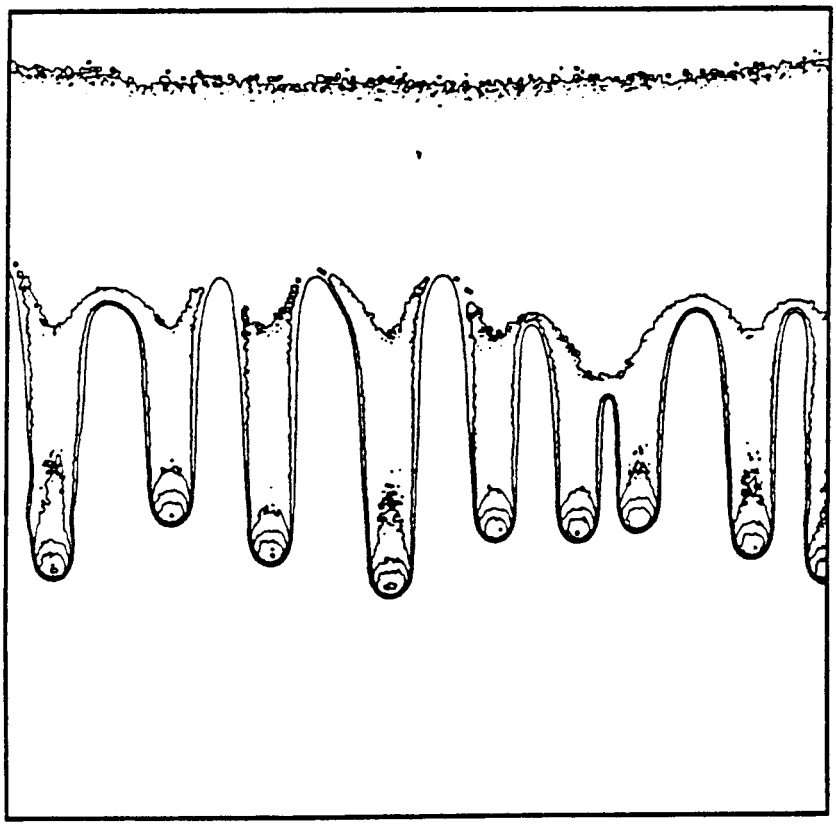

Fig. 9. Experimentally determined film thicknesses in the rivulet instability, as measured by transmission techniques. The figure shows contours of constant film thickness for glycerine, flowing down an inclined plane of glass under creeping flow conditions. From Goodwin (1991).

time of the rivulets in order to compute the capillary number Ca and therefore, the contact slope at the point of instability. We do this from the photographs shown in the papers. Huppert shows both chevron patterns for a silicone oil (Huppert, 1982, Fig. 1(c) and (d)), and straight rivulets for glycerine (Huppert, 1982, Fig. 1(g)), spreading on plexiglass. The onset time can be determined for the first case and estimated at 40s for the second. Silvi and Dussan V. (1991) also show photographs of chevrons for glycerine on glass (Silvi and Dussan V., 1991, Fig. 4(a)–(d), and straight rivulets for glycerine on plexiglass (Silvi and Dussan V., 1991, Fig. 4(e)–(h)). These figures have sufficient time resolution to allow a good estimate of the onset time and hence the capillary number at onset. From these estimates, we calculate that for Huppert's experiments $C = 0.05$ for silicone oil on plexiglass, and $C = 5$ for glycerine on plexiglass: for those of Silvi and Dussan V., $C = 0.8$ for glycerine on glass and $C = 7.0$ for glycerine on plexiglass. Thus we see that in all these experiments, the two chevron shapes always occurred for $C<1$, while the two straight-sided shapes always occurred for $C \gg 1$.

While the various experiments do not cover a systematic range of C, our simulations agree with all available experiments with regard to both the film profile and the mode of propagation.

4.3. Speculations regarding the mechanism

We interpret the existence of the two regimes and the parametric dependence of their existence in terms of the following physical mechanism. As we have seen, the contact line moves in response to the applied body force and the tendency of the evolution equation to produce regions of higher liquid level. This tendency in turn results from the dynamics in the underlying liquid, which are determined by a balance between viscous resistance, the driving body force, and the capillary pressure gradients associated with surface tension and interfacial curvature. In the case of large contact slope, the capillary pressure is capable of resisting the tendency of the fluid to spread laterally under the action of the driving force, since it can support relatively larger curvature. In one dimension, this gives rise to the well-studied increase of the height of the capillary ridge with increasing contact slope (Goodwin and Homsy, 1991; de Bruyn, 1992). In two dimensions, the ability of the interface to resist spreading forces is more profound, leading to the observed straight-sided rivulets. Once such a straight-sided rivulet is formed, it follows that the trough will tend to stop, since the flow driven by the body force is capable of entering the rivulet in a parallel flow consistent with the rivulet shape. The trough then feels no driving and adjusts to its equilibrium static shape. This situation cannot occur in the case of smaller contact slope, apparently because the capillary pressure cannot accommodate the transverse spreading forces. Spreading occurs continuously along the entire rivulet. The flux of fluid cannot be carried in a quasiparallel flow down the rivulet, and as a result significant driving persists at the troughs, causing them to continue to move.

Of course these comments are not an ab-initio explanation of the results, since they can only provide descriptive interpretations of the forces, given the rivulet shape. The latter is determined by the solution of the nonlinear moving boundary problem in which the shape and the flow are tightly coupled, and which must be solved numerically.

5. Summary and conclusions

We have developed a numerical algorithm capable of solving the moving boundary problem for one- and two-dimensional contact line motion for a general class of slip models. The algorithm was then applied to the problem of nonlinear rivulet instability for gravity driven flow down an inclined plate. Our conclusions can be summarized as follows:

1. There is only a small dependence of rivulet shape on the dimensionless slip parameter α over the range studied. This first conclusion suggests that nonlinear rivulet shape is relatively insensitive to the magnitude of the slip length and may even be insensitive to the details of the slip model used.
2. The main determinant of the rivulet shape is the numerical value of the contact slope, $C = (3Ca)^{-1/3}\tan(\theta)$, with chevron-shaped steady traveling waves occurring for $C<0.2$, convective chevron shapes for $0.2<C<1.0$, and straight-sided rivulets occurring for $C > 1.0$. This is the first study to establish the parametric dependence of nonlinear rivulet shapes on contact slope.
3. The predicted film profiles, shapes, and modes of propagation are in general agreement with

all available experiments. Our model, which assumes a constant contact angle and the simplest slip model that regularizes the contact line singularity, is capable of describing all known experimentally observed shapes. This suggests that more complex models, such as those involving the dynamic contact angle, are not necessary to do so. However, it may well be the case that dynamic contact angle models will be required to describe quantitatively the different flow regimes, especially at higher capillary number.

4. The nonlinear process by which either straight-sided or chevron-shaped rivulets are selected is rationalized in terms of the fundamental forces at play. For large C, the ability of the capillary pressure to withstand the lateral spreading forces, leads to a parallel flow within the straight-sided rivulet and the arresting of the motion of the trough. Conversely, for small C, the capillary pressure is too weak to resist the lateral spreading, with the result that the rivulet spreads laterally, the trough still feels a driving, and both peak and trough continue to move. What is remarkable is the establishment of equilibrium between lateral spreading rate and trough speed, leading to a steady traveling wave solution in the Lagrangian frame for small C.
5. Complete wetting of the substrate will occur, even in the presence of the rivulet instability, for $C<1.0$, as the troughs still move, albeit more slowly than the peaks. This observation is of obvious technological interest, and shows that complete wetting is a consequence of the *combination* of small contact angle and weak surface tension, (large Ca).

Acknowledgements

This work was completed as partial satisfaction of the MS degree requirements of DM and M.SC. GMH gratefully acknowledges the support of the US Department of Energy, Office of Basic Energy Sciences and in addition, thanks M. Pavletic and Prof. G. Yadigaroglu for their help in the editorial processing of this paper.

References

de Bruyn, J., 1992. Growth of fingers at a driven three-phase contact line. Phys. Rev. A 46, 4500–4503.

Fraysse, N., Homsy, G.M., 1994. An experimental study of rivulet instabilities in centrifugal spin coating of viscous Newtonian and non-Newtonian fluids. Phys. Fluids 6, 1491–1504.

Goodwin, R.T., III., 1991. An investigation of a viscous coating flow. PhD thesis, Department of Chemical Engineering, Stanford University.

Goodwin, R., Homsy, G.M., 1991. Viscous flow down a slope in the vicinity of a contact line. Phys. Fluids A 3, 515–528.

Greenspan, H.P., 1978. On the motion of a small viscous droplet that wets a surface. J. Fluid Mech. 84, 125–143.

Huppert, H., 1982. Flow and instability of a viscous current down a slope. Nature 300, 427–429.

Johnson, M.F.G., Schluter, R.A., Miksis, M.J., Bankoff, S.G., 1996. Experimental study of formation of rivulets from a constant flux fluid by fluorescence imaging at low Reynolds numbers. Applied Mathematics Technical Report 96-04. Department of Engineering Science and Applied Mathematics, Northwestern University.

Melo, F., Joanny, J., Fauve, S., 1989. Fingering instability of spinning drops. Phys. Rev. Lett. 63, 1958–1961.

Schwartz, L.W., 1989. Viscous flows down an inclined plane: instability and finger formation. Phys. Fluids A 1, 443–445.

Silvi, N., Dussan V., E., 1991. On the rewetting of an inclined solid by a liquid. Phys. Fluids 28, 5–7.

Spaid, M.A., Homsy, G.M., 1996. Stability of Newtonian and viscoelastic dynamic contact lines. Phys. Fluids 8, 460–478.

Spaid, M.A., Homsy, G.M., 1997. Stability of viscoelastic dynamic contact lines: An experimental study. Phys. Fluids 9, 823–832.

Troian, S., Herbolzheimer, E., Safran, S.A., Joanny, J.F., 1989. Fingering instabilities of driven spreading films. Europhysics Letters 10, 25–30.

Tuck, E.O., Schwartz, L.W., 1990. A numerical and asymptotic study of some third-order ordinary differential equations relevant to draining and coating flows. SIAM Rev. 32, 453–469.